

Amplitude-to-Phase Conversion in Injection-Locked CMOS Ring Oscillators

Zhaowen Wang

Abstract—Injection-locked ring oscillators (ILROs) are extensively employed for multi-phase clock generation in wireline and optical links. However, existing injection-locking theories primarily rely on linearized phase-domain or nonlinear time-domain models, which fail to account for amplitude-to-phase conversion effects inherent in ILROs. This paper introduces an enhanced analytical model based on an extension of Adler’s equation, explicitly incorporating amplitude-to-phase conversion. Simulation results demonstrate strong alignment with the proposed analytical predictions, validating the model’s accuracy in capturing the locking range and phasor relationships.

Index Terms—Wireline links, optical links, clocking, injection locking, ring oscillators, amplitude-to-phase conversion

I. INTRODUCTION

MULTI-phase clock generation finds many critical applications in high-speed communication systems, including multi-phase sampling, multi-phase receiver, digital transmitter, phase interpolation, phase array, frequency synthesis, and so on [1]–[8]. Injection-locked ring oscillators (ILROs) are widely used for multi-phase clock generation in high-speed wireline and wireless communications due to their symmetric structure, low jitter, and compact size [9], [10]. CMOS ILROs are particularly advantageous over their current-mode-logic (CML) counterparts due to their wider tuning range and lower jitter [11], [12]. However, a theoretical understanding of the injection lock mechanism in ILRO remains elusive.

Conventional injection-locking analyses include frequency-domain, time-domain, and phasor-domain approaches. Frequency-domain analysis, exemplified by Adler’s equation [13]–[15], was originally developed for harmonic oscillators, such as LC oscillators, where a resonator tank filters out harmonics and maintains a dominant fundamental tone, allowing for linear superposition. This method is unsuitable for ring oscillators, which lack such a tank and exhibit highly nonlinear waveforms.

Time-domain analysis models each ring oscillator stage as a linear RC filter with a hard-limiting transconductance [16], [17]. While this captures some transconductance nonlinearity, it neglects amplitude dependency. Furthermore, it better suits CML-based ROs, as CMOS ROs lack explicit RC filters.

Phase-domain response (PDR) analysis uses the impulse sensitivity function to model phase noise and locking range [18], [19]. While PDR captures the overall injection effect, it does not distinguish individual RO stages or analyze phase imbalance. Moreover, as a simulation-based approach, it offers limited design insights.

Several analytical models have been proposed for injection-locked ROs, but they are either too simplified to capture the amplitude dependency [20] or too complex to provide clear design insights [21].

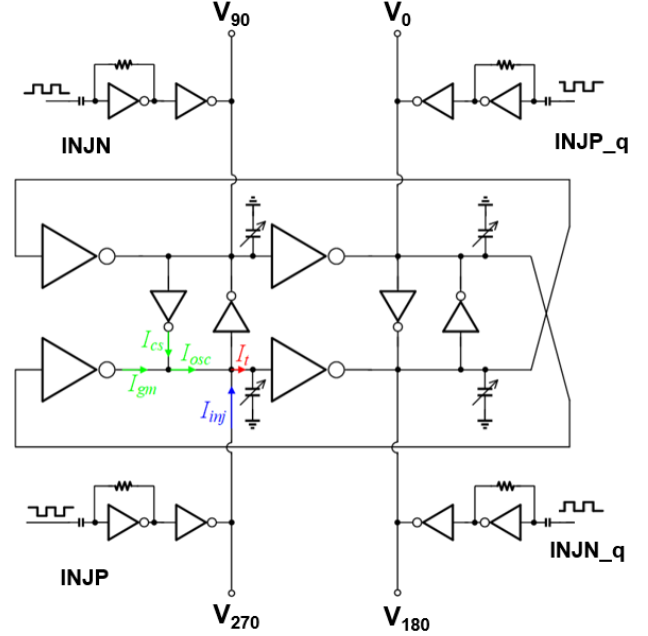


Fig. 1: The schematic diagram of an injection-locked ring oscillator with multi-phase injection.

This paper presents an extended Adler’s equation, a phasor-based analysis that incorporates amplitude dependency in CMOS ROs through amplitude-to-phase coefficients. Because CMOS ROs operate at high frequencies, their waveforms are still predominantly characterized by the fundamental frequency, making a phasor-based approach a reasonable approximation. The analytical results from the proposed model show good agreement with simulations, validating its effectiveness. This model provides new insights into the locking range, phase balance, and overall operation of ILROs.

The paper is organized as follows: Section II describes the CMOS RO model. Section III presents the extended model that incorporates amplitude to phase and compares the analytical and simulation results. Section IV concludes the paper.

II. CMOS RING OSCILLATOR MODELING

Even-stage CMOS ring oscillators (ROs) are commonly used for generating pseudo-differential clocks, so they will be the primary focus of this paper. Each stage employs a pair of cross-coupled inverters to ensure differential operation and suppress common-mode DC gain, preventing RO dead-lock (Fig. 1). Our RO model begins with a detailed modeling of a single stage.

A single RO stage comprises a differential input pair and a cross-coupled pair (Fig. 1). In a two-stage differential RO, the input to the first stage is 0° and 180° , producing outputs at 270° and 90° , respectively. The cross-coupled pair is driven

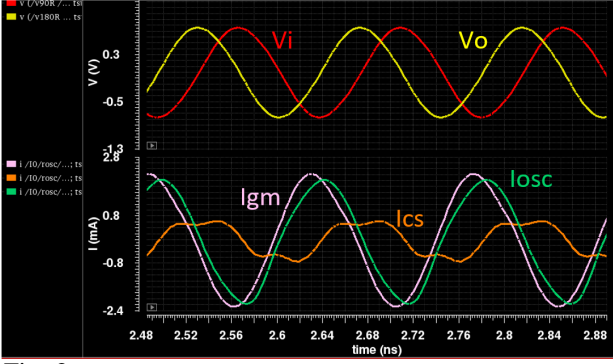


Fig. 2: The waveform of a 7-GHz free-running ring oscillator.

by these differential signals (e.g., 90° and 270° in the first stage). The main inverter generates a current phasor I_{gm} from V_0 , while the cross-coupled pair contributes a current phasor I_{cs} driven by V_{90} . The summation of these currents, i.e. I_{rosc} , results in a phase shift from I_{gm} , which is defined as θ_{VI} . In the two-stage differential RO, each stage needs to provide 90° phase shift, which is impossible through the conversion of current to voltage by first-order RC filtering. Thanks to the extra phase shift of θ_{VI} , the current-to-voltage conversion is less than 90° , which fulfills the oscillation requirement.

Fig. 2 shows the voltage and current waveforms of a free-running two-stage differential RO at 7GHz. Due to the high-frequency operation, the voltage waveform approximates a sinusoid. The main inverter, operating similarly to a class-AB amplifier, converts the input voltage into current. While it behaves as a hard current limiter at low speeds, it exhibits unity voltage gain in steady-state high-speed, high-swing operation. Its output current I_{gm} is predominantly the fundamental frequency. Moreover, the total current I_{osc} is shifted by the cross-coupled pair current I_{cs} , and it is still dominated by the fundamental tone. The current phase shift θ_{VI} is almost close to -5° , and the current-to-voltage conversion is around 85° , so the total single-stage phase shift is 90° . θ_{VI} and θ_{IV} are almost constant when the free-running frequency varies from 6 GHz to 8.5 GHz as shown by Fig. 3. Because the oscillation waveform is mostly dominated by the fundamental tone, a phasor-based analysis will be valid. In an eight-stage ring oscillator, the voltage waveform is closer to square waveform, and contains more high-order harmonics. Nevertheless, as the frequency is higher, its feedforward branch boosts the free-running frequency and also make its waveform more close to sinusoidal [22]. Therefore, in high-speed applications, phasor analysis still applies to 8-stage ROs.

Fig. 4 shows the phasor diagram in an RO. I_{gm} is the current driven by V_0 , θ_{VI} is the phase shift from the cross-coupled pair current I_{cs} . With injection locking, the injection current I_{inj} flows into the oscillation node, introduces an extra current summation and phase shift, and locks the RO to the injection frequency. In a multi-phase injection-locked RO, each oscillation node has its phase-shifted injection signals. ψ is the phase shift due to injection current I_{inj} , θ_{IV} is the phase shift from the current-to-voltage conversion, and the total current I_t generate the next-stage voltage V_{270} . ϕ_0 denotes the angle between I_{inj} and I_{osc} . In a multi-phase injection-locked case,

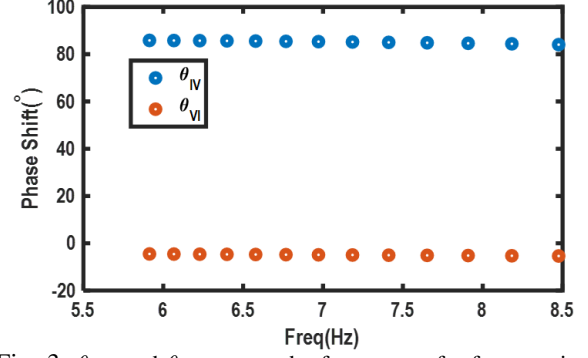


Fig. 3: θ_{IV} and θ_{VI} versus the frequency of a free-running ring oscillator.

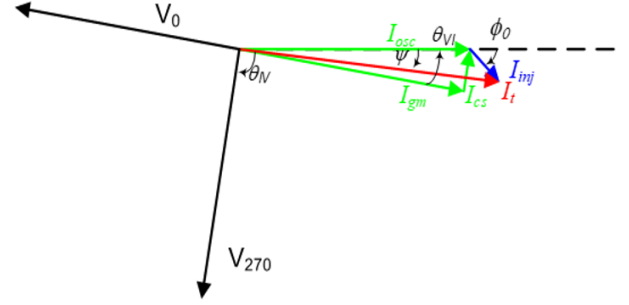


Fig. 4: The phasor diagram of the voltages and currents in an injection-locked ring oscillator.

V_0 and V_{90} have the same amplitude and have a quadrature relationship, and so do $I_{t,0}$ and $I_{t,90}$.

By sweeping the capacitor from 80 fF to 124 fF in the ring oscillator, its free-running frequency varies from 6 GHz to 8.5 GHz. Both θ_{IV} and θ_{VI} are independent from the free-running frequency, indicating a consistent behavior in the ring oscillator (Fig. 5). However, as the multi-phase injection enabled, only θ_{VI} varies against the free-running frequency, while θ_{IV} barely changes. Therefore, the angle of current-to-phase conversion θ_{IV} is almost a constant regardless of the injection conditions.

Fig. 6 further shows the phasor amplitude I_t and V_{osc} of the free-running and multi-phase injection locked RO. The free-running RO has a quite stable oscillation current and voltage amplitude while the injection-locked RO has a varying amplitude for either current or voltage. Moreover, the current reaches its maximum near the lower end of the locking range, while the voltage reaches its maximum near the higher end of the locking range.

Despite their nonlinear relationship with frequency, the voltage and current amplitudes exhibit a largely linear relationship, as shown in Fig. 6. Since the injection is typically designed to be between 0.05 and 0.2 of the main stage, it can be treated as a small signal. Consequently, the amplitude disturbance caused by the injection remains minimal. For instance, with an injection strength of 0.2, the amplitude varies only between 0.37 V and 0.45 V, representing approximately 20%. Thus, small-signal analysis can be effectively applied to study the sensitivity of the main stage and the cross-coupled pair [23], [24]. These components can be modeled as a combined transconductance stage with a phase shift, where the amplitude

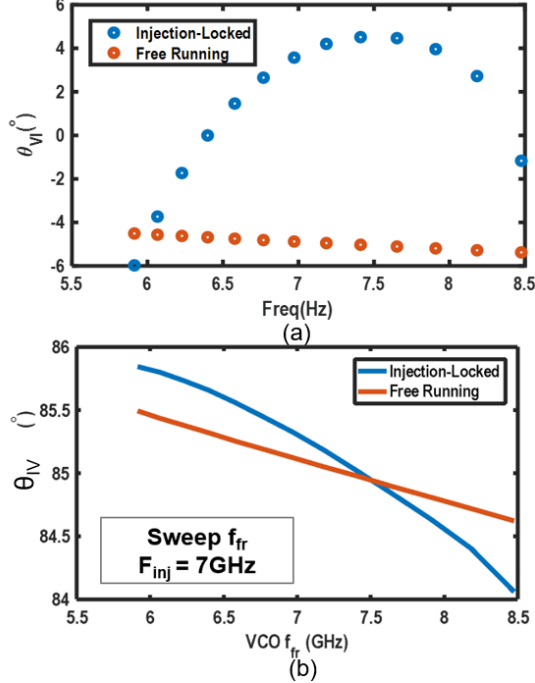


Fig. 5: θ_{IV} and θ_{VI} versus the free-running frequency of a ring oscillator with multi-phase injection enabled and disabled.

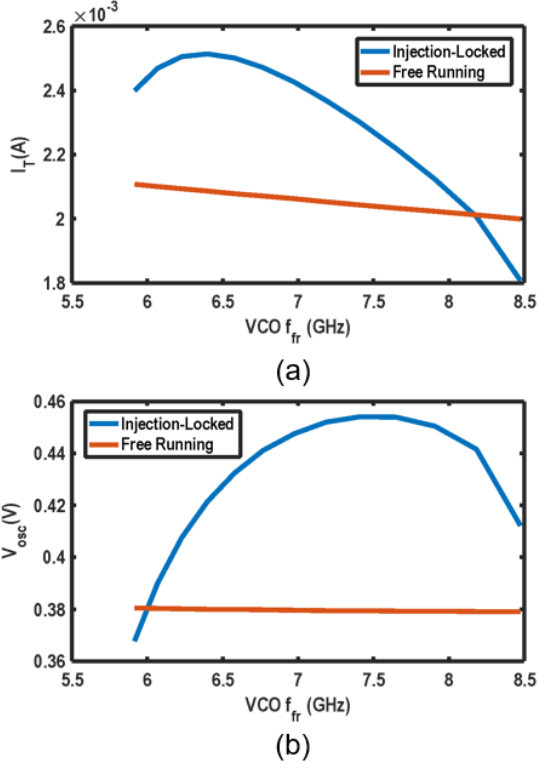


Fig. 6: the phasor amplitude I_t and V_{osc} in the RO with multi-phase injection enabled and disabled.

is represented by $I_{r_{osc}}$ and the phase shift by θ_{VI} . Using linear extrapolation, we derive the following equations, where A_{VI} and G_m are the current phase and amplitude sensitivity to its input voltage amplitude:

$$\theta_{VI} = A_{VI}|\vec{V}_{in}| + \theta_{VI,0} \quad (1)$$

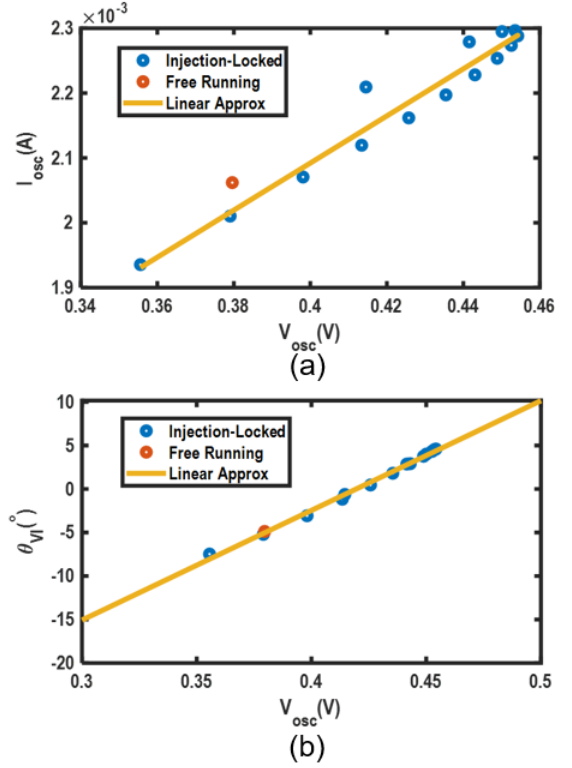


Fig. 7: The amplitude and phase of I_{osc} in the RO with multi-phase injection enabled and disabled.

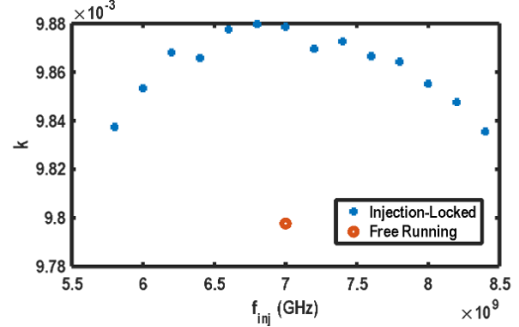


Fig. 8: k versus different injection frequencies.

$$|\vec{I}_{osc}| = G_m|\vec{V}_{in}| + I_{osc,0} \quad (2)$$

For the RO, the current-to-voltage delay of each stage can be expressed by $T_d = \theta_{IV}/(2\pi f)$. Alternatively, this delay can also be estimated by considering the time required to charge the total loading capacitance. In the steady state, the current and amplitude across the capacitor must satisfy the relationship $T_d = k*(CV_{osc})/I_t$, where k is a fixed coefficient accounting for the conversion from sinusoidal charging to linear current charging. From this, we can derive $k = I_t \times \theta_{IV} / (2\pi f V_{osc} C)$. Since k is a constant as shown by Fig. 9, the following equation holds true for oscillators both with and without injection:

$$\frac{|I_{osc,fr}| \theta_{IV,fr}}{C|V_{osc,fr}| f_{fr}} = \frac{|I_t| \theta_{IV,inj}}{C|V_{osc,inj}| f_{inj}} \quad (3)$$

We now have a model for the single stage in the ring oscillator (RO) that accounts for its amplitude dependency through the amplitude-to-amplitude coefficient G_m and amplitude-to-

phase coefficient A_{VI} . This model can be seamlessly incorporated into Adler's equation.

III. EXTENDED ADLER'S EQUATION WITH AMPLITUDE-TO-PHASE CONVERSION

A. Adler's Equation

Adler's equation describes injection locking by analyzing the summation of current phasors [13]. The oscillator's current phasor is I_{osc} , and the injection current phasor is I_{inj} . The total current is shifted by an angle of ψ from I_{osc} due to the influence of I_{inj} . In the conventional analysis, When I_t is orthogonal to I_{inj} , ψ reaches its maximum at $\arctan(I_{inj}/I_{osc})$. This relationship is instrumental in analyzing the locking range, noise sensitivity, and other characteristics of an injection-locked oscillator. For an N-stage multi-phase injection-locked RO, Adler's equation can be expressed as:

$$\vec{I}_{osc} + \vec{I}_{inj} = \vec{I}_t \quad (4)$$

$$\theta_{VI} + \psi - \theta_{IV} = \pi/N \quad (5)$$

$$\frac{\theta_{VI,fr}}{f_{fr}} = \frac{\theta_{VI,inj}}{f_{inj}} \quad (6)$$

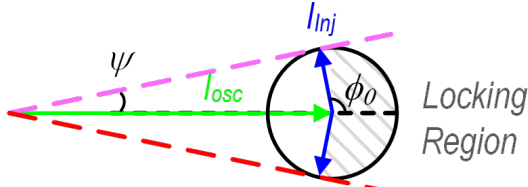


Fig. 9: Phasor diagram for Adler's equation.

B. Extended Adler's Equation

To extend Adler's equation by incorporating amplitude-to-phase conversion, Equations 1 and 2 are introduced. Injection locking alters the total current amplitude, necessitating adjustments to the model. As a result, the complete set of equations can be expressed as:

$$\vec{I}_{osc} + \vec{I}_{inj} = \vec{I}_t \quad (7)$$

$$\theta_{VI} + \psi - \theta_{IV} = \pi/N \quad (8)$$

$$\frac{|\vec{I}_{osc,fr}| \theta_{VI,fr}}{V_{osc,fr} f_{fr}} = \frac{|\vec{I}_t| \theta_{VI,inj}}{V_{osc} f_{inj}} \quad (9)$$

$$\theta_{VI} = A_{VI} |\vec{V}_{in}| + \theta_{VI,0} \quad (10)$$

$$|\vec{I}_{osc}| = G_m |\vec{V}_{in}| + I_{osc,0} \quad (11)$$

$$\phi_0 = -\angle \vec{I}_{inj} \quad (12)$$

$$\psi = -\angle \vec{I}_t \quad (13)$$

Unlike the symmetric locking range predicted by the conventional Adler's equation, the extended equation accounts for amplitude-to-phase conversion, resulting in an asymmetric locking range. Additionally, the phasor diagram demonstrates a varying amplitude, as illustrated in Fig. 10.

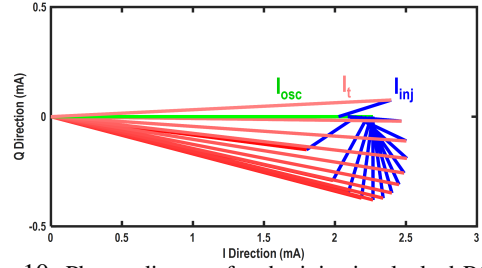


Fig. 10: Phasor diagram for the injection-locked RO with amplitude-to-phase conversion.

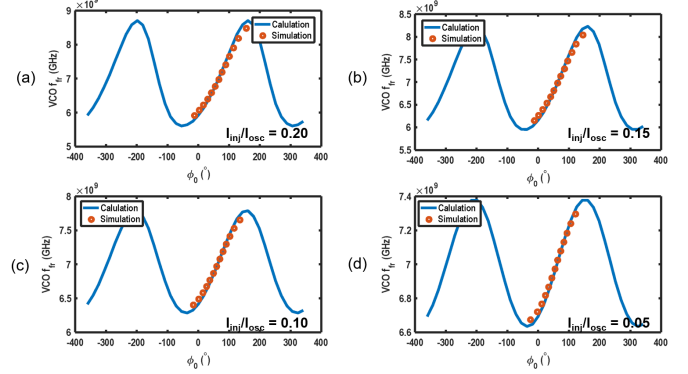


Fig. 11: Calculated and simulated ϕ_0 versus free-running frequency under injection strength: (a) 0.2; (b) 0.15; (c) 0.10; (d) 0.05.

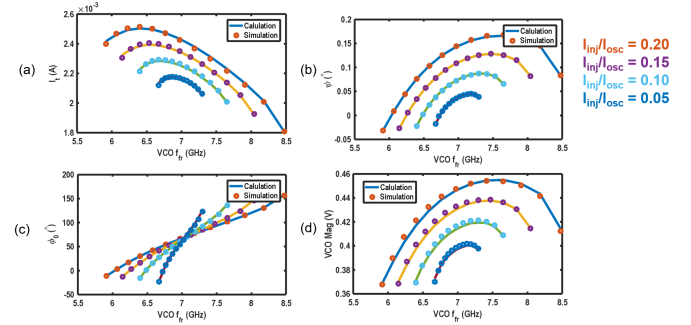


Fig. 12: Calculated and simulated $I_t, \psi, \phi_0, V_{osc}$ versus free-running frequency under injection strength: (a) 0.2; (b) 0.15; (c) 0.10; (d) 0.05.

C. Analytical and Simulation Results

We examine the equations using a two-stage multi-phase injection-locked ring oscillator.

First, the injection frequency is fixed at 7 GHz, and the free-running frequency is swept under varying injection strengths of 0.05, 0.10, 0.15, and 0.20. As shown in Fig. 11, the equations provide analytical solutions for ϕ_0 , which correspond to specific locking ranges for each injection strength. The results indicate a wider locking range at the high-frequency end and a narrower range at the low-frequency end. Fig. 12 compares the current amplitude, ϕ_0 and ψ , and oscillation amplitude across the free-running frequency for different injection strengths. The extended equations accurately predict these values, validating the amplitude-to-phase conversion effect in injection-locked oscillators.

Next, we fix the free-running frequency at 7 GHz and sweep the injection frequency under varying injection strengths of 0.05, 0.10, 0.15, and 0.20. As shown in Fig. 13, the equations provide analytical solutions for ϕ_0 , corresponding to

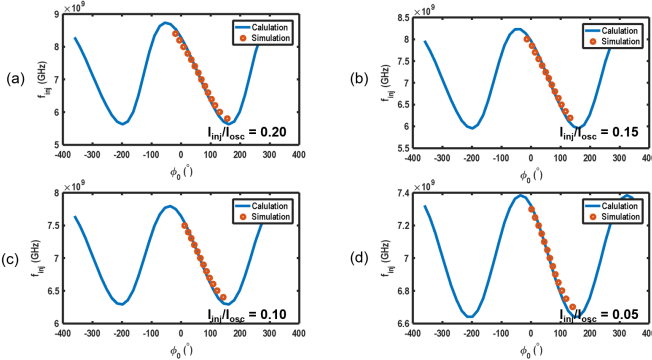


Fig. 13: Calculated and simulated ϕ_0 versus injection frequency under injection strength: (a) 0.2; (b) 0.15; (c) 0.10; (d) 0.05.

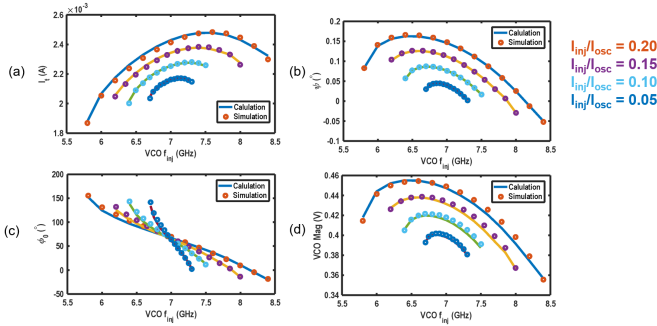


Fig. 14: Calculated and simulated $I_t, \psi, \phi_0, V_{osc}$ versus injection frequency under injection strength: (a) 0.2; (b) 0.15; (c) 0.10; (d) 0.05.

specific locking ranges for each injection strength. The results demonstrate a wider locking range at the high-frequency end and a narrower range at the low-frequency end. Fig. 14 compares the current amplitude, ϕ_0 and ψ , and oscillation amplitude across the injection frequency for different injection strengths. The extended equations accurately predict these values, further validating the amplitude-to-phase conversion effect in injection-locked oscillators.

IV. CONCLUSIONS

This paper presents an enhanced analytical model that extends Adler's equation by accounting for amplitude-to-phase conversion. Simulation results show excellent agreement with the analytical predictions, confirming the model's accuracy in capturing the locking range and phasor dynamics. The proposed equations effectively describe the phase and amplitude relationships in injection-locked ring oscillators and can be further extended to predict phase noise sensitivity through small-signal analysis.

REFERENCES

- [1] Z. Wang, "Efficient and high-performance clocking circuits for high-speed data links," Ph.D. dissertation, Columbia University, New York, 2022.
- [2] S. Chen *et al.*, "A 4-to-16GHz inverter-based injection-locked quadrature clock generator with phase interpolators for multi-standard I/Os in 7nm FinFET," in *IEEE Int. Solid-State Circuits Conf. Dig. Tech. Papers (ISSCC)*, San Francisco, CA, USA, Feb. 2018, pp. 390–392.
- [3] C. Poon *et al.*, "A 1.24pJ/b 112Gb/s (870Gbps/mm) transceiver for in-package links in 7nm FinFET," in *Proc. Symp. VLSI Circuits*, Kyoto, Japan, Jun. 2021, pp. 1–2.

- [4] Z. Wang and P. R. Kinget, "A 65nm CMOS, 3.5-to-11GHz, less-than-1.45LSB-INL_{ppp}, 7b twin phase interpolator with a wideband, low-noise delta quadrature delay-locked loop for high-speed data links," in *IEEE Int. Solid-State Circuits Conf. Dig. Tech. Papers (ISSCC)*, San Francisco, CA, USA, Feb. 2022, pp. 292–294.
- [5] H. Xu, J. Bi, T. Zou, W. He, Y. Zeng, J. Gu, Z. Jiao, S. Liu, Z. Zhu, and N. Yan, "5.1 A 5-to-16GHz reconfigurable quadrature receiver with 50% duty-cycle LO and IQ-leakage suppression," in *2024 IEEE International Solid-State Circuits Conference (ISSCC)*, San Francisco, CA, USA, Feb. 2024, pp. 88–90.
- [6] J. Li, Z. Li, Y. Yin, C. Yan, N. Qi, M. Liu, and H. Xu, "4.4 a highly-integrated 6-phase cell-reused digital transmitter using 1/3 duty-cycle LO signals for harmonic rejection," in *2024 IEEE International Solid-State Circuits Conference (ISSCC)*, San Francisco, CA, USA, Feb. 2024, pp. 82–84.
- [7] Z. Wang, H. Jiang, and P. R. Kinget, "A digital pre-distortion technique for high-linearity, low-power, compact, phase interpolators," in *2024 IEEE International Symposium on Circuits and Systems (ISCAS)*, Singapore, Singapore, 2024, pp. 1–5.
- [8] Z. Wang and P. R. Kinget, "A very high linearity twin phase interpolator with a low-noise and wideband delta quadrature DLL for high-speed data link clocking," *IEEE J. Solid-State Circuits*, pp. 1172–1184, 2023.
- [9] P. Kinget *et al.*, "An injection-locking scheme for precision quadrature generation," *IEEE Journal of Solid-State Circuits*, vol. 37, no. 7, pp. 845–851, Jul. 2002.
- [10] Z. Wang *et al.*, "11.4 A high-accuracy multi-phase injection-locked 8-phase 7GHz clock generator in 65nm with 7b phase interpolators for high-speed data links," in *IEEE Int. Solid-State Circuits Conf. Dig. Tech. Papers (ISSCC)*, San Francisco, CA, USA, Feb. 2021, pp. 186–188.
- [11] A. Abidi, "Phase noise and jitter in CMOS ring oscillators," *IEEE J. of Solid-State Circuits*, vol. 41, no. 8, pp. 1803–1816, Aug. 2006.
- [12] Z. Wang *et al.*, "Multi-phase clock generation for phase interpolation with a multi-phase, injection-locked ring oscillator and a quadrature DLL," *IEEE J. Solid-State Circuits*, pp. 1776–1787, 2021.
- [13] R. Adler, "A study of locking phenomena in oscillators," *Proceedings of the IRE*, vol. 34, no. 6, pp. 351–357, Jun. 1946.
- [14] B. Razavi, "A study of injection locking and pulling in oscillators," *IEEE Journal of Solid-State Circuits*, vol. 39, no. 9, pp. 1415–1424, Sep. 2004.
- [15] D. Yang, A. Abidi, H. Darabi, H. Xu, D. Murphy, H. Wu, and Z. Wang, "16.6 a calibration-free triple-loop bang-bang pll achieving 131firms jitter and-70dbc fractional spurs," in *2019 IEEE International Solid-State Circuits Conference - (ISSCC)*, Feb. 2019, pp. 266–268.
- [16] G. Gangasani and P. Kinget, "A time-domain model for predicting the injection locking bandwidth of nonharmonic oscillators," *IEEE Transactions on Circuits and Systems II: Express Briefs*, vol. 53, no. 10, pp. 1035–1038, Oct. 2006.
- [17] —, "Time-domain model for injection locking in nonharmonic oscillators," *IEEE Transactions on Circuits and Systems I: Regular Papers*, vol. 55, no. 6, pp. 1648–1658, Jul. 2008.
- [18] A. Hajimiri and T. Lee, "A general theory of phase noise in electrical oscillators," *IEEE J. of Solid-State Circuits*, vol. 33, no. 2, pp. 179–194, Feb. 1998.
- [19] B. Hong and A. Hajimiri, "A phasor-based analysis of sinusoidal injection locking in lc and ring oscillators," *IEEE Transactions on Circuits and Systems I: Regular Papers*, vol. 66, no. 1, pp. 355–368, Jan. 2019.
- [20] M. Raj *et al.*, "22.3 A 4-to-11GHz injection-locked quarter-rate clocking for an adaptive 153fJ/b optical receiver in 28nm FDSOI CMOS," in *IEEE Int. Solid-State Circuits Conf. Dig. Tech. Papers (ISSCC)*, San Francisco, CA, USA, Feb. 2015, pp. 1–3.
- [21] Y. Zhang, Z. Wang, and P. R. Kinget, "Analysis of injection-locked ring oscillators for quadrature clock generation in wireline or optical transceivers," *IEEE Trans. Circuits Syst. I*, vol. 69, no. 8, pp. 3074–3082, Aug. 2022.
- [22] I.-F. Sun *et al.*, "A comparative study of 8-phase feedforward-coupling ring vcos," *IEEE Transactions on Circuits and Systems II: Express Briefs*, vol. 66, no. 4, pp. 527–531, Apr. 2019.
- [23] D. Auvergne *et al.*, "Signal transition time effect on CMOS delay evaluation," *IEEE Trans. Circuits Syst. I*, vol. 47, no. 9, pp. 1362–1369, Sep. 2000.
- [24] A. Kabbani *et al.*, "Technology-portable analytical model for dsm cmos inverter transition-time estimation," *IEEE Transactions on Computer-Aided Design of Integrated Circuits and Systems*, vol. 22, no. 9, pp. 1177–1187, Sep. 2003.